UNSTEADY MODEL OF SAIL AND FLOW INTERACTION

O. Le Maître, S. Huberson

*Laboratoire de Mécanique, Université du Havre BP 540,
76 058 Le Havre, France*

AND

E. Souza De Cursi

*INSA de Rouen, Département de Mécanique Place E. Blondel,
76 000 Mont Saint Aignan, France*

We present an analysis and a numerical method for predicting the response of a two-dimensional sail in unsteady flow. The fluid is considered inviscid and incompressible so that the perturbation of the uniform inflow can be treated within vortex sheet theory. Due to the very small thickness of the sail, the assumption of the ideal flexibility can be made, and a nonlinear membrane model is used to solve the dynamics of the sail. Energy considerations on the complete system provide a variational formulation of the flow-structure interaction problem, which can be solved by using the boundary element method and a point vortex approximation of the wake. Numerical simulations for harmonic perturbation of the trailing edge and random inflows exhibit the nonlinear response of the sail. © 1999 Academic Press

1. INTRODUCTION

MANY PRACTICAL SITUATIONS INVOLVE FLUID–STRUCTURE interactions, namely, the coupling between a flowing fluid and an elastic structure. Such a situation is very often found in engineering applications and has been studied extensively in the literature. The most usual approach for this situation introduces two distinct problems that one can consider as 'tasks': (i) the fluid task is to determine the flow for given boundary conditions; the resolution of this initial/boundary value problem allows the evaluation of the forces applied by the fluid on the structure (here the sail); (ii) the structural task is to analyse the behaviour of the sail for a given history of the external forces. These tasks are not independent: the fluid applies forces on the sail and generates deformation and motion. So, the displacements of the fluid–solid interface generate a perturbation of the flow. In fact the motion of the sail is coupled to the flow. As a consequence, the resolution of the interaction requires the simultaneous resolution of both tasks.

In this work, we consider the interaction of a yacht sail with an incompressible flow, but the theory and the methodology can easily be extended to other very thin and flexible structures, such as soft wings and parachutes. In most situations, sail operate in a natural environment characterized by unsteadiness and complex perturbations (atmospheric turbulence and complete motions of the yacht caused by sea-wave excitation). Figure 1 schematically presents the sources of excitation that induce unsteadiness in yacht aerodynamics.
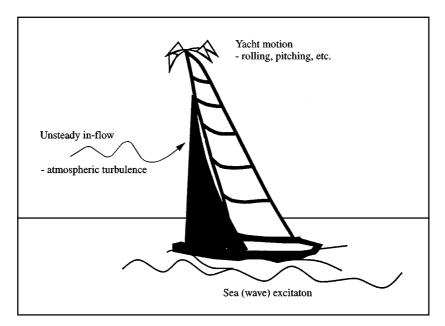
Figure 1. Schematic representation of sailing yacht problem. Unsteadiness emerges from perturbations of the in-flow (turbulent, wind, gusts) and of the ship motion mainly induced by waves.

Then, a model of interaction for complex boundary conditions is of interest for anyone concerned with design and efficient prediction. Current numerical investigations of sail response to flow interaction mainly deal with steady problems [see Jackson *et al.* (1985, 1986) and Fukasawa & Katori (1992)], and unsteady computations of flows around sails assume rigid motions of the structures [see, for example, Charvet (1992) and Flay (1997) for a general overview of recent work on sail aerodynamics]. Nevertheless, shape variations and elastic deformations of the sail can strongly affect the complete dynamics of the system, but the resolution of the interaction involves many geometrical difficulties connected to large displacements and nonlinearities.

In order to overcome such difficulties, several simplifications can be found in the literature: asymptotic analysis of the flow, e.g. prescribed wake, lifting-line theory, camber effects, etc. (Abbot & Von Doenhoff 1958; Guermond & Sellier 1991; Wilmott 1988; Katz & Plotkins 1991), linear elastic model of deformation displacements from rigid or mean shape (Zienkiewicz 1977; Batoz & Dhatt 1992; Bernadou 1994), and approximation of the coupling equations on the undeformed shape (Dowell *et al.* 1978; Bisplinghoff & Ashley 1982). The approach consisting in the geometrical linearization of the fluid solid interface was shown to be effective for calculations for many situations, but for large displacements of the interface such linearizations can lead to erroneous results [see, e.g. Charvet *et al.* (1994) and Bréard (1996)]. In fact, the problem is weakly nonlinear, irrespective of the fluid and solid mechanical models. Moreover, functional resolution requires complex procedures in order to avoid any time shift between the solutions in the solid and fluid domains.

The objective of this work is to determine the essential phenomena appearing in unsteady fluid–structure interactions, and we focus on large displacement effects. In this way, we analyse the two-dimensional problem of an ideally flexible sail set in a uniform inflow. This problem is illustrated in Figure 2.

In Section 2, a model for the flow field is introduced. For inviscid fluid, a small angle of attack, and in the limit of a zero thickness obstacle, the flow around the sail is kinematically
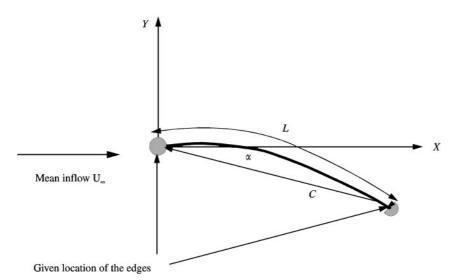
Figure 2. Schematic representation of the problem studied. A flexible sail of natural length L is set in a uniform in-flow. Motion of the edges is prescribed and the angle of attack α is small. Distance between the edges is denoted by C.

equivalent to the flow induced by a bound vortex sheet merged with the mean line of the obstacle and by the wake [see Rosenhead (1931), Saffman (1992) and Leonard (1980)]. This representation supposes that the flow remains attached along the sail so that the bound sheet is continuously linked to the wake at the trailing edge (this is an equivalent form of the Joukovski condition). The wake contains the information concerning the time-history of the system and can be treated within the context of vortex sheet theory (Rosenhead 1932; Leonard 1980). The history of the system is recorded in the wake by irreversible transfer of circulation from the boundary layer of the obstacle to the wake according to Kelvin's theorem (Batchelor 1967). Moreover, vortex sheet theory provides an integral expression for the velocity and kinetic energy of the flow field from the configurations (position) of the obstacle and wake vortex sheet and from their circulation (Saffman 1992).

In Section 3 the energies of the elastic sail are presented. We consider a sail of constant thickness h and natural length $L \gg h$. Here, natural length should be understood as measured on a zero strain configuration (which is not necessarily unique). The solid domain is mapped on $\mathscr{S} = [0:L] \times [0:h] = \mathscr{L} \times [0:h]$. If the thickness h is very small compared to L, the structure can be considered as a one-dimensional medium and its actual configuration is known by a map $\mathbf{x}_B$ of the mean line which associates a Lagrangian coordinate $l \in \mathscr{L}$ to a position:

$$l \in \mathscr{L} \Rightarrow \mathbf{x}_B(l) \in \mathbb{R}^2. \tag{1}$$

For very small thickness, the elastic energy of the structure is only a function of the mean line configuration. As previously stated, only the kinetic and elastic energies of the sail are of interest. These energies can easily be estimated from a geometrically nonlinear membrane model: the elastic energy is a quadratic form of the strains of the mean line, while the kinetic energy of the sail is a quadratic function of the derivative of $\mathbf{x}_B$ with respect to time.

Given these different expressions for the kinetic and elastic energies of the sail, as well as the kinetic energy of the flow, it is possible to apply variational principles to characterize the complete system. This analysis is developed in Section 4. It is based on the principle of

minimum of energy in the system and it leads to a variational equation, the unknown being the configuration $\mathbf{x}_B$ at every time. An analysis of the resulting variational equation in terms of fluid characteristic scales leads to the characterization of the interaction by three-dimensional parameters. The first two parameters respectively compare elastic stresses to the fluid pressure and the inertia of the sail to the inertia of the fluid, while the last parameter reflects the ability of the sail to undergo large displacements.

A discretization of the variational equation is then proposed in Section 5. It involves a hybrid aeroelastic finite-element approximation of the obstacle and a particle representation of the wake (Katz & Plotkins 1991). The time discretization is performed by means of a Runge–Kutta scheme for the kinematic field in the solid domain and for the computation of the wake particle trajectories.

Sections 6 and 7 are devoted to numerical results obtained with the model. First, the influence of the system parameters on the response is investigated for harmonic perturbations of the trailing edge location. This computational case is an idealization of the situation for which the motion of the yacht is the combination of translation and rolling motions. Finally, a random perturbation analysis is used to predict the response of the system to complex external, forcing, including many time modes, and to investigate the influence of the sail characteristics. Random analysis is necessary, because sails usually operator in various conditions which are sometimes unpredictable.

General conclusions on this work are presented in Section 8, as well as a discussion on the extension of the model to three-dimensional flows.

2. THE FLOW MODEL

2.1. BOUNDARY CONDITIONS FOR THE FLOW

For an inviscid two-dimensional flow, natural boundary conditions for the velocity are the slip-stream condition on $\delta\Omega$ and the undisturbed inflow at infinity. The first condition states the continuity of the normal components of the fluid and solid velocities on the sail surface. In the limit of a zero thickness sail, this kinematic boundary condition is written on the sail mean line $\mathscr{L}$ as

$$\mathbf{U}(\mathbf{x}_B) \cdot \mathbf{n} = \frac{\mathrm{d}\mathbf{x}_B}{\mathrm{d}t} \cdot \mathbf{n}, \tag{2}$$

where $\mathbf{n} = \mathbf{k} \times \partial_l \mathbf{x}_B / |\partial \mathbf{x}_B|$ is the normal ($\mathbf{k}$ being the unitary vector normal to the plane of the study), $\mathbf{U}$ is the velocity, and ∂_l stands for $\partial/\partial l$. The set, $\mathscr{V}$ of admissible fluid velocity fields is

$$\mathscr{V} = \{\mathbf{V} | \nabla \cdot \mathbf{V}, \text{ equation } (2)\}, \tag{3}$$

where $\mathbf{V}$ is the nabla operator: $\mathbf{V}^{\mathrm{T}} = \{\partial/\partial x, \quad \partial/\partial y\}$.

As a consequence of the slip-stream condition, the flow field can only admit a tangential discontinuity, ΔU. We have

$$\Delta U(l) = (\mathbf{U}^-(\mathbf{x}_B(l)) - \mathbf{U}^+(\mathbf{x}_B(l))) \cdot (\mathbf{n} \times \mathbf{k}),$$

where the superscripts $+$ and $-$ stand for the upper and lower sides of the sail.

This discontinuity of the tangential velocity is equivalent to a vortex sheet [see Saffman (1992) and Katz & Plotkins (1991)] merged with $\mathbf{x}_B$. The circulation per unit length $\gamma_B(l)$

carried by the arc-length element δl of the sail is denoted by $\gamma_B(l)$ and is given by (Saffman 1992)

$$\gamma_B(l) \approx \Delta U(\mathbf{x}_B).$$

The conservation of the circulation in the fluid domain is a well known result of vortex dynamics (Batchelor 1967). Let $\Gamma_B(t)$ be the total circulation of the sail,

$$\Gamma_B(t) = \int_0^L \gamma_B(l) \, \mathrm{d}l,$$

and Γ_ω be the circulation in the wake. Since the total circulation remains constant, we have

$$\frac{\mathrm{d}\Gamma_\omega}{\mathrm{d}t} = \tilde{\gamma}_\omega(t) = -\frac{\mathrm{d}\Gamma_B}{\mathrm{d}t}. \tag{4}$$

This constraint is physically satisfied by shedding vorticity in the fluid at the trailing edge, as described later.

2.2. WAKE DYNAMICS

The vorticity-velocity formulation of the momentum equation is obtained by taking the curl of Euler equation. For inviscid 2-D flow, we have:

$$\frac{\mathrm{d}\omega}{\mathrm{d}t} = 0, \tag{5}$$

where $\omega = \mathbf{V} \times \mathbf{U}$ is the vorticity.

Equation (5) shows that the vorticity contained in any volume of fluid is kept constant. Thus, it is possible to model the wake as a singular distribution of vorticity along a thin line, namely a vortex sheet. This strip evolves with the flow, and the circulation $\delta\gamma_\omega$ carried by the strip length material element $\delta\tau$ does not vary with time. Thus, the wake is approximated by a material line carrying a circulation distribution and moving with the local fluid velocity, which in turn depends on the circulation distribution. The wake is described in terms of a map $\mathbf{X}_\omega$ which associates a position to the Lagrangian coordinate $\tau \in [0; t]$. The governing equations of the wake are summarized by

$$\mathbf{X}_\omega(\tau, t = \tau) = \mathbf{x}_B(l = L, t = \tau), \tag{6a}$$

$$\gamma_\omega(\tau)|_{t=\tau} = -\frac{\mathrm{d}\Gamma_B}{\mathrm{d}t}\bigg|_{t=\tau}, \tag{6b}$$

$$\frac{\mathrm{d}}{\mathrm{d}t} \int_{\delta l_\omega} \gamma_\omega(\tau) \, \mathrm{d}\tau = 0, \tag{6c}$$

$$\frac{\mathrm{d}\mathbf{X}_\omega}{\mathrm{d}t} = \mathbf{U}(\mathbf{X}_\omega). \tag{6d}$$

Here δl_ω is a material line (wake) element. Equation (6a) is the consequence of prescribing the shedding point at the trailing edge: the sail and the wake are continuously linked at the trailing edge. The second equation, (6b), relates changes in the circulation of the bound and free vortex sheets and ensures the conservation of the total circulation. Equations (6c) and (6d) are Euler's equation written in a characteristic form: the circulation carried by a material line element is kept constant and is convected by the flow.

2.3. VELOCITY FIELD AND KINETIC ENERGY

Using Green's functions, the stream function of the flow can be written in terms of the circulation distributions over the sail and the wake:

$$\psi(\mathbf{x}') = \frac{1}{4\pi}\left[\int_{\mathscr{L}} \gamma_B(l)\ln(|\mathbf{x}_B - \mathbf{x}'|)\,\mathrm{d}l + \int_0^t \gamma_\omega(\tau)\ln(|\mathbf{X}_\omega - \mathbf{x}'|)\,\mathrm{d}\tau\right] + \psi_\infty(\mathbf{x}'), \qquad (7)$$

where ψ_∞ is the incident flow stream function. This equation provides an explicit expression for $\mathbf{U}$:

$$\mathbf{U}(\mathbf{x}', t) = \nabla \times \psi = \frac{1}{4\pi}\left[\int_{\mathscr{L}} \frac{\gamma_B(l)\mathbf{k} \times (\mathbf{x}' - \mathbf{x}_B)}{|\mathbf{x}' - \mathbf{x}_B|^2}\,\mathrm{d}l + \int_0^t \frac{\gamma_\omega(\tau)\mathbf{k} \times (\mathbf{x}' - \mathbf{X}_\omega)}{|\mathbf{x}' - \mathbf{X}_\omega|^2}\,\mathrm{d}\tau\right] + \mathbf{U}_\infty. \quad (8)$$

The Kinetic energy in an unbounded domain, can be expressed in terms of stream function and vorticity,

$$2\mathscr{K}(t) = \rho \iint_\Omega \psi\omega\,\mathrm{d}\mathbf{x}\,\mathrm{d}\mathbf{x}' = -\rho \int_{\mathscr{L}} \psi\,\gamma_B\,\mathrm{d}l - \rho \int_0^t \psi\gamma_\omega\,\mathrm{d}\tau, \qquad (9)$$

where ρ is density of the fluid. Substituting equations (8) and (7), and using equation (6), the rate of change of kinetic energy is equal to

$$\frac{\mathrm{d}\mathscr{K}}{\mathrm{d}t} = \rho \int_0^L \frac{\mathrm{d}\gamma_B}{\mathrm{d}t}\,\psi\,\mathrm{d}l + \rho \int_0^L (\gamma_B\,\mathbf{k} \times \mathbf{U}(\mathbf{x}_B)) \cdot \frac{\mathrm{d}\mathbf{x}_B}{\mathrm{d}t}\,\mathrm{d}l.$$

Alternatively, $\psi(l)$ can be written as

$$\psi(\mathbf{x}_B(l)) = \psi(\mathbf{x}_B(0)) + \int_0^l (\mathbf{U}(\mathbf{x}_B(l')) \cdot \mathbf{n})\,\mathrm{d}l'.$$

The stream function can be chosen such that $\psi(\mathbf{x}_B(0)) = 0$. By doing so, and using equation (2), we finally obtain

$$\frac{\mathrm{d}\mathscr{K}}{\mathrm{d}t} = \rho \int_0^L \left[\int_0^l \frac{\mathrm{d}\gamma_B(l')}{\mathrm{d}t}\,\mathrm{d}l'\right]\frac{\mathrm{d}\mathbf{x}_B}{\mathrm{d}t} \cdot \mathbf{n}\,\mathrm{d}l + \rho \int_0^L (\gamma_B\mathbf{k} \times \mathbf{U}(\mathbf{x}_B)) \cdot \frac{\mathrm{d}\mathbf{x}_B}{\mathrm{d}t}\,\mathrm{d}l. \qquad (10)$$

Alternatively, the rate of change of kinetic energy can be written as

$$\frac{\mathrm{d}\mathscr{K}}{\mathrm{d}t} = \rho \iint_\Omega \mathbf{U} \cdot \frac{\mathrm{d}\mathbf{U}}{\mathrm{d}t}\,\mathrm{d}\mathbf{x} = \iint_\Omega -\mathbf{U} \cdot (\nabla P)\,\mathrm{d}\mathbf{x} = -\int_{\delta\Omega} P(\mathbf{U} \cdot \mathbf{n})\,\mathrm{d}\mathbf{x},$$

where P is the total head. The right-hand-side term of the previous expression is the power of the normal load applied by the fluid on the obstacle ($P \cdot \mathbf{n}$). Since $\mathbf{U} \cdot \mathbf{n}$ is continuous across both sides of the sail, the previous expression can be re-written introducing the pressure jump $\Delta P = P^+ - P^-$ across the sail:

$$\frac{\mathrm{d}\mathscr{K}}{\mathrm{d}t} = -\int_0^L \Delta P \frac{\mathrm{d}\mathbf{x}_B}{\mathrm{d}t} \cdot \mathbf{n}\,\mathrm{d}l.$$

It is now easy to relate the pressure jump, ΔP, to the loads on the obstacle by using equation (10):

$$\Delta P = \rho \int_0^l \frac{\mathrm{d}\gamma_B(l')}{\mathrm{d}t}\,\mathrm{d}l' + \rho[\gamma_B\mathbf{k} \times \mathbf{U}(\mathbf{x}_B)] \cdot \mathbf{n}. \qquad (11)$$

The first term in equation (11) is the unsteady load, the second term is the steady equivalent body force acting on the fluid [see also Katz & Plotkins (1991) and Batchelor (1967)]. The influence of the history on the dynamics of the system appears in equations (10) and (11) through **U**, which involves an integration along the wake.

3. THE ELASTIC SAIL MODEL

3.1. STRAINS AND TENSIONS

For very thin and flexible structures, the mechanical behaviour in the solid domain $\mathscr{S}$ can be approached by using a large-displacement membrane model. The solid domain has been considered as one-dimensional, so that the state of the structure (kinetic energy, internal stresses) is a function of the mean line configuration $\mathbf{x}_B$. As a consequence, this model neglects the variations in the thickness direction. Moreover, if the thickness h is small compared to the local radii of curvature, flexural stresses can be neglected too, leading to ideally flexible behaviour, where only strains of the mean line are taken into account in the deformation. More details of the elastic analysis are available in Antman (1995), and only the main results are reported in the following.

If the Lagrangian coordinate l is also a measure of the natural arc-length, the local strain is given by

$$\varepsilon(l) = |\partial_{,l}\mathbf{x}_B| - 1. \tag{12}$$

In this work, only materials for which the tension Λ can be approximated by a linear function of the strain (small strain rates), have been considered:

$$\Lambda(l) = E_y \varepsilon(l), \tag{13}$$

where E_y is Young's modulus of the material. For ideally flexible behavior, the field of tension $\mathbf{\Lambda}$ in the sail is tangential to the mean line (Antman 1995):

$$\mathbf{\Lambda}(l, \eta) = \Lambda \partial_{,l}\mathbf{x}_B / |\partial_{,l}\mathbf{x}_B| = E_y \varepsilon \partial_{,l}\mathbf{x}_B / |\partial_{,l}\mathbf{x}_B|, \quad \forall \eta \in [0:h]. \tag{14}$$

The boundary conditions for the solid problem are given by the kinematics of the sail edges ($\mathbf{x}_B(l=0) = \mathbf{x}_0(t)$ and $\mathbf{x}_B(l=L) = \mathbf{x}_L(t)$). We define the set of admissible configurations $\mathscr{C}$ by

$$\mathscr{C} = \{\mathbf{y}(l) \mid \mathbf{y}(0) = \mathbf{x}_0(t), \quad \mathbf{y}(L) = \mathbf{x}_L(t), \quad \forall t > 0\}.$$

3.2. ENERGIES OF THE STRUCTURE

To construct a variational problem for the interacting system, we are concerned with the kinetic energy T of the structure and its elastic potential Θ.

The kinetic energy of the sail is a quadratic functional of the velocity:

$$2T = \int_{\mathscr{L}} \rho_s h \left[\frac{d\mathbf{x}_B}{dt}\right]^2 dl, \tag{15}$$

where ρ_s is the density of the undeformed structure.

For a member model, the elastic potential (or elastic energy) of the sail associated with the configuration $\mathbf{x}_B$ is a quadratic functional of the strains:

$$2\Theta = \int_{\mathscr{L}} hE_y[\varepsilon]^2 \, \mathrm{d}l. \tag{16}$$

The sum of the elastic potential and solid kinetic energy can be differentiated with time to provide the instantaneous variations of the structure energy:

$$\frac{\mathrm{d}(T + \Theta)}{\mathrm{d}t} = \int_{\mathscr{L}} h \left[\mathbf{\Lambda} \cdot \partial_{,l} \frac{\mathrm{d}\mathbf{x}_B}{\mathrm{d}t} + \rho_s \frac{\mathrm{d}^2\mathbf{x}_B}{\mathrm{d}t^2} \cdot \frac{\mathrm{d}\mathbf{x}_B}{\mathrm{d}t} \right] \mathrm{d}l. \tag{17}$$

4. COMPLETE AEROELASTIC MODEL

The variations of the energy of the complete system (i.e. in the fluid and solid domain) can be estimated from the previous elementary models. Let J be this instantaneous rate of change,

$$J(\mathbf{x}_B) \equiv \frac{\mathrm{d}(\mathscr{K} + T + \Theta)}{\mathrm{d}t}. \tag{18}$$

Application of variational principles on the system energy states leads to the following optimization problem:

Problem 1. Find, for every time t, the configuration $\mathbf{x}_B \in \mathscr{C}$ which minimizes J given by equation (18).

A variational formulation of Problem 1 is Problem 2 as follows:

Problem 2. Find $\mathbf{x}_B \in \mathscr{C}$ such that

$$\int_{\mathscr{L}} \left[\left(\int_0^l \rho \frac{\mathrm{d}\gamma_B(l')}{\mathrm{d}t} \, \mathrm{d}l' \right) \mathbf{n} + \rho(\gamma_B \mathbf{k} \times \mathbf{U}(\mathbf{x}_B)) + h \left(\mathbf{V} \cdot \partial_{,l} + \rho_s \frac{\mathrm{d}^2\mathbf{x}_B}{\mathrm{d}t^2} \right) \right] \cdot \mathbf{V}^* \, \mathrm{d}l = 0, \quad \forall \mathbf{V}^* \in \mathscr{D}, \tag{19}$$

where $\mathscr{D} = \{y \,|\, y(0) = 0, \, y(L) = 0\}$ is the set of admissible virtual velocities ($\mathbf{V}^*$) of the sail mean line. In equation (19), γ_B is such that the total velocity $\mathbf{U}$ given by equation (8) satisfies the boundary conditions on the sail ($\mathbf{U} \in \mathscr{V}$), and $\mathbf{\Lambda}$ is given by (14). We shall assume that the solution of Problem 2 exists and is unique.

A dimensionless form of Problem 2 is obtained by considering the characteristic length L, and velocity U_∞ of the free stream. The characteristic time and load (stress) of the interaction then are

$$t_c = L/U_\infty, \quad P_c = \rho U_\infty^2.$$

Introducing these characteristic quantities into equation (19) yields two dimensionless parameters. The first one, denoted P_s, is the ratio of the characteristic elastic stress to the characteristic fluid stagnation pressure, while the second, P_m, is the ratio of inertial forces in the two domains:

$$P_s = hE_y/\rho LU_\infty^2, \quad P_{m,} = h\rho_s/L\rho.$$

For a sail, we can expect P_m to vary from ≈ 0 (light materials and large yacht) to $0 \cdot 5$ (dinghies and heavy fabrics). P_s can take values over a much larger range, because for a given sail it is a function of the in-flow (wind) velocity U_∞ which depends on weather conditions. Usually, extreme values for U_B are estimated to be 0 (no-wind) and 30 m s^{-1} (≈ 60 knots). For common sails, the order of magnitude for $E_y h$ is 10^6 Pa m, so we can

expect P_s to vary from 100 [very windy and large yachts (sails)] to ∞ (no wind and dinghies).

Another important parameter, which characterizes the sail geometry, is defined as the ratio of the natural length of the structure, L to the distance, C, between its edges; it is a measure of the natural curvature. When $L/C > 1$ natural configurations (unstrained) are not unique and for every admissible configuration there exist many displacement fields that conserve the elastic energy Θ, so that a better adaptation of the sail to external loads can be expected compared with the case where $L/C \leq 1$. This parameter will be referred to as P_g.

5. DISCRETISATION OF PROBLEM 2

5.1. FLOW PROBLEM

The solution of Problem 2 involves two main difficulties connected with the computation of the flow fields for a given history of the configuration, on the one hand, and the resolution of equation (19), on the other. For a given history of the deformation, the distribution of circulation density is the solution of an unsteady boundary value problem at every time step: γ_B is such that the slip-stream condition equation (2) is satisfied. Because of the conservation of the total circulation, equation (4), this problem is not linear: the boundary conditions of the problem depend on γ_B through the velocity field $\mathbf{U}$, which is also a function of the shed circulation given by equation (4). Moreover, the time integration of the wake equation has to be performed at the same time. Many procedures can be found in the literature to solve this problem, and we choose to adapt the method developed in Charvet *et al.* (1992, 1997) for three-dimensional flows. This method combines a point vortex method (Leonard 1980) for the wake discretization with a lifting surface model (Katz & Plotkins 1991) for the sail. Simplification of the models for a two-dimensional problem is straightforward (Le Maître *et al.* 1997a) and is not detailed here.

5.2. DISCRETIZATION OF THE VARIATIONAL PROBLEM

Using the implicit, second-order, Runge–Kutta scheme, we can write the velocity and acceleration fields as linear functions of their values at the previous time step and of $\mathbf{x}_B(t + \Delta t)$ the unknown solution. Introducing this time discretization in equation (19), the following problem is obtained: to find $\mathbf{x}_B(t + \Delta t)$ such that

$$\int_{\mathscr{L}} [\mathbf{F}(t + \Delta t) + h\mathbf{\Lambda}(t + \Delta t) + h\beta_a \rho_s \mathbf{x}_B(t + \Delta t)] \mathbf{V}^* \, \mathrm{d}l = -\int_{\mathscr{L}} h\rho_s \mathbf{A}^P(\mathbf{x}_B(t), \dot{\mathbf{x}}_B(t)) \mathbf{V}^*, \quad \forall V^* \in \mathscr{D}, \tag{20}$$

where $\mathbf{A}^P$ is a function of the configuration and its velocity at the previous time step, β_a is a coefficient which only depends on Δt and $\mathbf{F}(t + \Delta t) = \Delta P \mathbf{n}$ is the aerodynamic load [equation (1)]. This equation is approximated using a finite element method (Zienkiewicz 1977) which results in a nonlinear system of equations in the discrete degrees of freedom of the sail centreline, $\{\mathbf{x}_{Bi}\}_{i=1}^{N}$: Let $\varXi$ be the resulting system of nonlinear equations for the $\mathbf{x}_{Bi}$:

$$\varXi(\mathbf{x}_{Bi}(t + \Delta t)) = 0. \tag{21}$$

Then, equation (21) can be solved by successive approximations as described in the next subsection.

5.3. Iterative Algorithm

Some difficulties arise when solving system Ξ because of the strong non linearities of the equations relative to $\mathbf{x}_B(t + \Delta t)$. Nevertheless, the solution can be obtained by cyclic iterations, starting from a guess solution $\mathbf{x}_g$. The iterations are as follows

(i) $\mathbf{x}_g$ is used to estimate $\mathbf{F}$ and $\mathbf{\Lambda}$ on the obstacle. The estimation of $\mathbf{F}$ involves the resolution of the fluid problem, as discussed in Section 5.1.

(ii) Estimate the residue $\mathbf{R}(\mathbf{x}_g)$ of the set of nonlinear equations: $\Xi(\mathbf{x}_g) = \mathbf{R}(\mathbf{x}_g)$

(iii) Relaxation of the solution:

$$\mathbf{x}_g \leftarrow \mathbf{x}_g + \mu\mathbf{R}(\mathbf{x}_g).$$

Estimate the convergence. Let $R^2 = |\mathbf{R}(\mathbf{x}_g)|$ be the norm of the residue of system Ξ for the tested solution $\mathbf{x}_g$. If R^2 is smaller than a prescribed parameter then the solution $\mathbf{x}_g$ is considered accurate, otherwise a new cycle is performed starting from step. (i).

(iv) The solution is updated:

$$\mathbf{x}_B(t + \Delta t) = \mathbf{x}_g.$$

Numerical integration of the wake equation (6d) over the time step.

(v) A new time iteration can begin at step (i), providing an estimation $\mathbf{x}_g$ for $\mathbf{x}_B(t + 2\Delta t)$, and so on.

In this scheme, μ is a (small) relaxation parameter that is chosen to ensure convergence of the $\mathbf{x}_g$ series to the solution.

6. HARMONIC PERTURBATION OF THE TRAILING EDGE

6.1. Selection of the Numerical Parameters

We present results obtained for the resolution of the dimensionless variational problem. Thus, all quantities appearing in the following sections are dimensionless with respect to the selected characteristic scales of the problem: L, U_∞ and ρ. The two edges of the sail are separated by a constant distance which is P_g^{-1}. Because of the fluid model, which assumes that the flow is attached along the obstacle, the angle of attack has to remain moderate during computations in order to avoid any separation of the flow.

The computations are used to determine the response of the system to a uniform in-flow, and a perturbation of the trailing edge location (i.e. a perturbation of the angle of attack) is analysed. Thus, the sail boundary conditions are chosen as follows:

$$\mathbf{x}(l = 0) = \mathbf{x}_0 = \begin{Bmatrix} 0 \\ 0 \end{Bmatrix}, \quad \mathbf{x}(l = L) = \mathbf{x}_L = \begin{Bmatrix} P_g^{-1} \cos \alpha \\ -P_g^{-1} \sin \alpha \end{Bmatrix}, \tag{22}$$

where $\alpha(t)$ is the angle of attack of the obstacle and obeys

$$\alpha(t) = \bar{\alpha} + \alpha_{TE} \cos \omega_{TE} t. \tag{23}$$

Here ω_{TE} is the angular velocity of the trailing edge, $\bar{\alpha}$ is the mean angle of attack and α_{TE} the amplitude of the trailing edge perturbation. As previously discussed, the applications of the model are restricted to moderate angles of attack and ω_{TE} because the flow is assumed to remain fully attached along the sail.

This harmonic disturbance of the trailing edge can be interpreted as an approximation of real sailing conditions. For example, one can imagine the case of a yacht cruising on a wavy
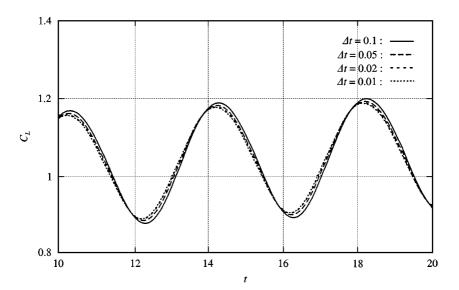
Figure 3. Evolution of lift coefficient C_L with time for different time steps Δt. For the computations $P_m = 0.1$, $P_s = 250$, $\alpha_{TE} = 2°$, $\tilde{\alpha} = 15°$ and $\omega_{TE} = \pi/2$ rad.

sea which comes up against the swell with a frequency f_w, so that the reduced angular velocity of the perturbation can be estimated as

$$\omega_{TE} = 2\pi f_w L / U_\infty.$$

Since f_w is nearly constant for given sea conditions (neglecting variations of the absolute yacht velocity), the corresponding angular velocity is a function of the relative wind velocity U_∞ and can reach large values when U_∞ is small.

The sail is spatially discretized using a number of boundary element, denoted by N_ε, equal to 15, and we set $P_g = 1$. The system is then fully defined by ω_{TE}, $\tilde{\alpha}$, P_s and P_m.

The effect of the time step is first studied. Figure 3 shows signals for the lift coefficient, C_L, for different time-steps. The lift coefficient represents the resulting load applied by the fluid on the sail in the direction normal to the free stream:

$$C_L = \left\| \int_0^1 \left[\left(\int_0^l \frac{d\gamma_B}{dt} \, dl' \right) \mathbf{n} + \gamma_B \mathbf{k} \times \mathbf{U}(\mathbf{x}_B) \right] \times \mathbf{U}_\infty \, dl \right\|.$$

These results show that $\Delta t = 0.02$ is sufficiently small to obtain an accurate solution, at least for the tested angular frequency of the trailing edge. As the computation begins from steady state (impulsively started obstacle), it can be noticed that the periodic behaviour is still not reached at time $t = 20$ and the mean C_L still slowly increases. The wake has to expand over a long length downstream, before a periodic state is reached. From the computational cost point of view, it must be noted that $\Delta t \approx 0.01$ is an acceptable value. For a large number n of time steps, the computational cost for the wake evolution increases as n^2, so it is of interest to minimize the number of time steps necessary for large time analysis. On a HP 712/100 workstation, a simulation over 8000 time steps lasts about 20 h and corresponds to a relative translation of perturbation and C_L response becomes larger, and lower frequency modes in the lift coefficient signal appear (see Figures 4 and 5).
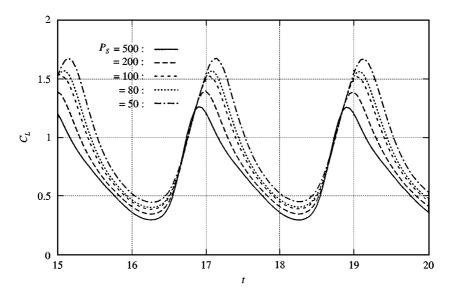
Figure 4. Evolution of C_L with time for different load parameters P_s; $\Delta t = 0 \cdot 02$, $\bar{\alpha} = 10°$, $\alpha_{TE} = 2°$, $P_m = 0 \cdot 1$, $\omega_{TE} = \pi$ rad, $P_g = 1$.

6.4. INFLUENCE OF ω_{TE}

The previous results show that when P_m takes moderate values, the leading effect on the sail response is the transfer of vorticity, i.e. of energy, from the obstacle to the wake. Next, we investigate the effect of the nonlinear wake dynamics by increasing progressively the trailing edge pulsation, so that the energy transfer increases. In this way, we fix $N_\varepsilon = 10$, $\Delta t = 0 \cdot 01$, $P_m = 0 \cdot 1$, $P_s = 500$, $\alpha_{TE} = 2°$ and $\bar{\alpha} = 10°$ and we test the following values for ω_{TE}: 1, 2, 4, 6 and 8 (in radians). To underline nonlinear effects, we took $P_g = 1 \cdot 02$, so that the sail admits natural curvature which favour intense vortex shedding. Again, the nonlinear coupling between the structure and the flow is quite obvious from the C_L signals which are plotted in Figure 6. Low-frequency perturbations induce a nearly linear response, whereas large frequencies lead to very complex ones (see $\omega_{TE} = 8$ rad for instance).

In Figure 7 we compare the different spectra of the C_L signals. In this plot, we have used the reduced frequency F^*, which is the ratio of the dimensionless frequency of the signals with perturbation frequency $f_p = \omega_{TE}/2\pi$. These spectra show the different behaviours depending on the frequency of the perturbation. For low frequency, the system responds at the same frequency. As ω_{TE} increases, the energy of the C_L signal becomes distributed over harmonics and subharmonics of the perturbation. For $\omega_{TE} = 8$, the C_L spectrum presents a much more dispersed energy distribution with many significant frequencies. It is worthwhile to note that the computation of the spectra has been performed with a fast Fourier transform algorithm over 4096 time steps, representing a time simulation extending over more than a hundred periods of perturbation when $\omega_{TE} = 8$. Data are recorded only 20 perturbation periods after the simulation started in order to minimize the effect of the impulsive start.

7. RANDOM PERTURBATIONS

7.1. DEFINITION OF IN-FLOW DISTURBANCE

The analysis of the response in terms of harmonic perturbations is not, generally, adapted to deal with nonlinear coupling between different modes of perturbation. Moreover, in real
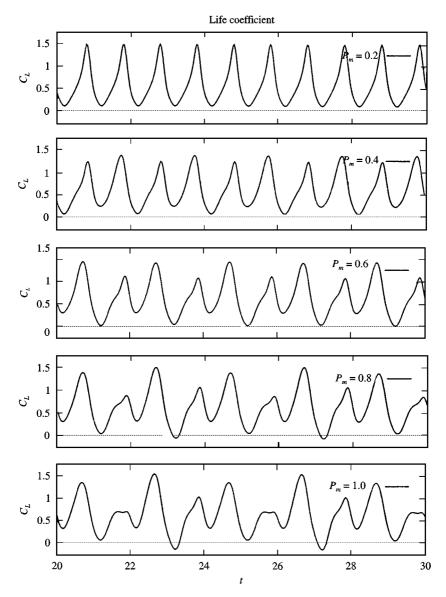
Life coefficient

Figure 5. Lift coefficient C_L as a function of time t and for $P_m = 0.2$, 0.4, 0.6, 0.8 and 1.0; $\bar{\alpha} = 10°$, $\alpha_{TE} = 2°$, $P_s = 500$, $P_g = 1$, $N_e = 10$, $\Delta t = 0.03$, and $\omega_{TE} = 2\pi$ rad.

life, sails, and other structures such as delta wings and para-gliders, are submitted to complex inflows (due to atmospheric turbulence for instance) or complex motion of the complete crew (when maneuvering or due to wave perturbation for a yacht) and are supposed to operate under various wind conditions.

Random simulation is one alternative to overcome the difficulty in the definition of realistic boundary conditions and in the analysis of a nonlinear coupling between frequencies. We present in this section the analysis of the interaction of a sail with fixed edges in an unsteady random inflow. The free stream is defined by a mean velocity U_∞ (the wind) and an unsteady perturbation $U'(t)$. The angle between the chord of the obstacle (the line which links the two edges) and the in-flow direction is α and is assumed to be small.
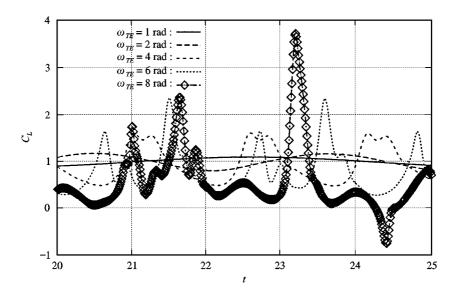
Figure 6. Time evolution of the lift coefficient signals for different pulsations of the trailing edge perturbation. Computational parameters are $N_e = 10$, $\Delta t = 0{\cdot}01$, $P_m = 0{\cdot}1$, $P_s = 500$, $\alpha_{TE} = 2°$ and $\bar{\alpha} = 10°$.
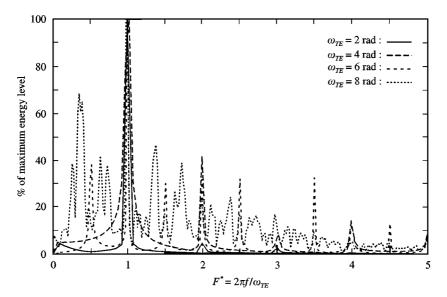

Figure 7. Spectra of the lift coefficient signals for different pulsations of the trailing edge perturbation. Computational parameters are $N_e = 10$, $\Delta t = 0{\cdot}01$, $P_m = 0{\cdot}1$, $P_s = 500$, $\alpha_{TE} = 2°$ and $\bar{\alpha} = 10°$.

In order to build realistic random perturbations of the in-flow, it is first necessary to define the statistical characteristics of the perturbations. Here measurements are required, but very few exist (especially measurement of atmospheric turbulence over seas). Because our model is limited to irrotational and incompressible inflows we assume the characteristic length scale of perturbations is large compared to L. Then, the perturbations $U'(t)$ can be considered uniform in space, and the resulting inflow is a uniformly pulsed flow; we have
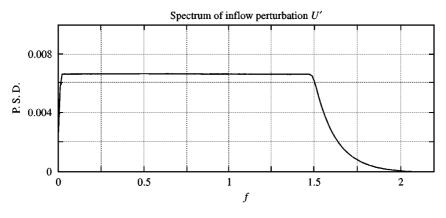
$$\mathbf{U}_{fs}(t) = (U_\infty + U'(t))\mathbf{i},$$

Figure 8. Spectrum of the perturbation of the in-flow velocity, U'.

where $\mathbf{U}_{fs}$ is the instantaneous free-stream velocity. The aim of the present simulations is to analyse the system response for successive increasing and decreasing velocity of the in-flows (namely gusts). The effects of atmospheric turbulence on the wake development are not taken into account here (Bréard 1996), because the perturbations are simply transported with a variable but uniform velocity.

A basic model for the wind perturbations considered can be defined from a mean velocity, a variance, and an energy spectrum in the frequency domain. The mean wind velocity U_∞ can easily be estimated, but the variance of U_{fs} depends on many factors: roughness of the sea, height above sea-level, air characteristics, local effects, etc. The same difficulty arises with velocity spectra which can vary a great deal from one site to another. Despite the lack of statistical data, it is possible to find in the literature some orders of magnitude for velocity variance in atmospheric boundary layer, and for frequency ranges with significant energy (see for instance Kree & Soize 1984). Accordingly, we choose for the computation a variance equal to 0·01 for the dimensionless velocity of the free-stream. According to Kree & Soize (1984), the highest frequency to be considered in atmospheric boundary layer is 2 Hz, and we selected a spectrum which is flat for the range of reduced frequencies between 0 and 1·5, and decreases exponentially to 0 for reduced frequencies higher than 2·5. The corresponding spectrum is plotted in Figure 8. It should be underlined that when perturbations of the motion of the complete structure are considered (for example in the case of a yacht response to random waves excitations) corresponding spectra would probably differ and exhibit some discrete frequencies, much more than continuous spectra. From the perturbation spectrum, it is possible to build a random time series using random phase and inverse Fourier transform. An example of the resulting time series for the velocity is presented in Figure 9.

7.2. Influence of P_m on the Response to Random Perturbations

First, we set the numerical parameters to $N_e = 10$, $\Delta t = 0·02$, the angle of attack $\alpha = 10°$, $P_s = 500$ and we observe the dependence of the computed spectrum of the lift coefficient on the mass parameter P_m. Five values for P_m have been tested: 0·1, 0·2, 0·4, 0·6 and 0·8. Two cases have been distinguished according to whether P_g is greater than 1 or not. In subsection 7.2.1, we analyse the response of the system for $P_g = 0·99$ and the defined random perturbations. In subsection 7.2.2, we study the case where the structure presents a natural curvature: $P_g = 1·02$.
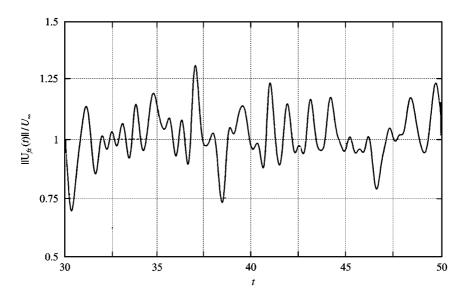
Figure 9. Example of random velocity inflow evolution with time. The variance of this signal is 0·01 and its mean value is 1.

TABLE 1

C_L mean value and variance for various values of the mass parameter P_m and $P_g = 0.99$. P_s is fixed equal to 500 and $\alpha = 10°$. Numerical parameters are $\Delta t = 0.02$ and $N_e = 10$. Variance of the dimensionless in-flow velocity is 0·01 and its spectrum is reported in Figure 8

P_m	0·1	0·2	0·4	0·6	0·8
C_L mean	0·597	0·596	0·596	0·595	0·595
C_L variance	0·0549	0·0462	0·0339	0·0264	0·0221

7.2.1. $P_g = 0.99$ — *Random perturbations*

For P_g lower than 1, no admissible configuration corresponds to a natural configuration (zero strain). The sail is strained even if fluid loads are removed. In Table 1 we report the variances and the mean values of the C_L signals for the different mass parameter values.

Table 1 shows that the mean value of C_L is unaffected by P_m, but that the variance of C_L is strongly affected by P_m. As P_m increases, the variance of the lift coefficient decreases. Thus, it appears that increasing the inertia of the sail penalizes its displacements and deformations, which consequently reduces shape variations.

The effect of increasing P_m is also visible in the spectra of C_L signals, which are plotted in Figure 10. Each curve is computed from 4096 data points. Examination of these spectra clearly demonstrates the nonlinear behaviour of the system by comparing the different kinds of spectra of the external forcing and of the response: when the energy of the forcing is equally distributed over the range $f \in [0, 1.5]$, the response spectra exhibits energy peaks at particular frequencies. Actually, it is well known that such a nonlinear system filters the perturbations and responds to characteristic frequencies often called wetted frequencies. These results also show that as P_m increases the maximum energy level decreases and the peak moves to the lower side of the frequency domain. It confirms the observation of
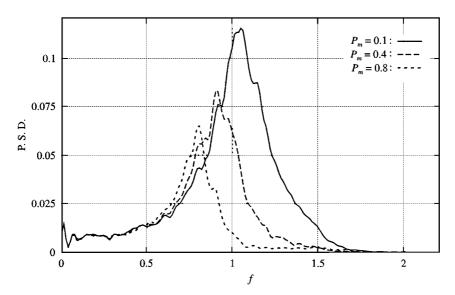
Figure 10. Spectra of C_L signals for random perturbations of the inflow and for different values of P_m. Numerical parameters are $N_e = 10$, $\Delta t = 0.02$, and the system is defined by $\alpha = 10°$, $P_s = 500$ and $P_g = 0.99$.
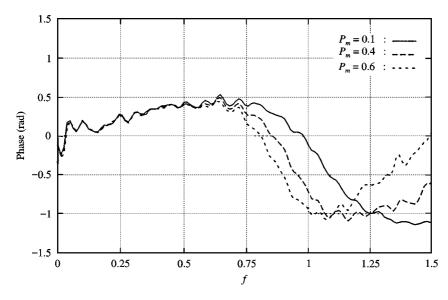

Figure 11. Phase shift between C_L signals and inflow perturbation signal in the frequency domain. Parameters of the system are given in Figure 10.

Table 1: for increasing inertia of the sail, high-frequency modes of shape deformation are penalized, and the same phenomenon occurs for the loads. In Figure 11 we plot the corresponding phase shifts between the lift coefficient C_L and the in-flow perturbation. The phase shift between response and perturbation is very interesting in design when studying the stability and control of the system. Results show that the phase shift is nearly unaffected by P_m variation for low frequencies (≤ 0.75). However, the shift appears to become negative as soon as P_m increases.

TABLE 2

C_L mean value and variance as a function of P_m for $P_g = 1.02$. Dimensionless variance of the inflow perturbations is 0.01 and its spectrum is given in Figure 9. System parameters are $P_g = 1.02$, $P_s = 500$ and $\alpha = 10°$. Numerical parameters are $N_e = 10$, $\Delta t = 0.02$.

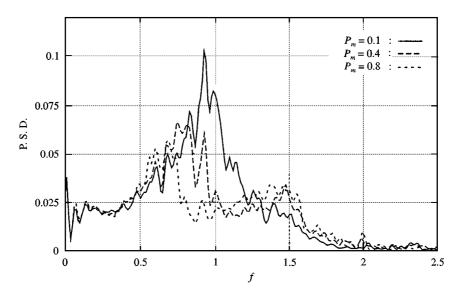| P_m	0.1	0.2	0.4	0.6	0.8
C_L mean	0.99	1.00	1.00	1.00	1.00
C_L variance	0.0605	0.0556	0.0524	0.0499	0.0484

Figure 12. Spectra of C_L signal for random perturbations defined in previous section. Parameters of the system are $N_e = 10, \Delta t = 0.02$, the angle of attack α is taken equal to $10°$, $P_s = 500$ and $P_g = 1.02$.

7.2.2. $P_g = 1.02$ — *Random perturbations*

Now the natural length L of the structure is larger than the distance C between the two edges. Thus, there exist many natural configurations, and large displacements can easily be realized. The main effect appearing when increasing P_g from 0.99 to 1.02, can be seen in Table 2, which must be compared with Table 1 (other parameters are kept unchanged).

As expected, the length excess favours the displacements and curvatures for equivalent strain rates and then higher mean C_L than for pre-strained case of the previous subsection. Variance is also affected by the ability of the structure to bend: C_L signals exhibit greater variance when P_g is greater than 1, but this variance is also penalized by the structure inertia (when P_m increases). Figure 12 shows the corresponding spectra. It is noted that, contrary to the case with $P_g = 0.99$, the system now responds to every excitation frequency, even to the highest, for which the energy remains significant when $P_m = 0.8$. Nevertheless, the system still exhibits a preferential frequency range, as manifested by the dependence of the maximum energy peak on P_m. Again, the maximum energy frequency decreases as well as the maximum of energy when P_m increases, and the spectra become flatter. Computations also demonstrate a very different behaviour from the previous case in terms of phase shift for frequencies higher than 1 (see Figure 13).
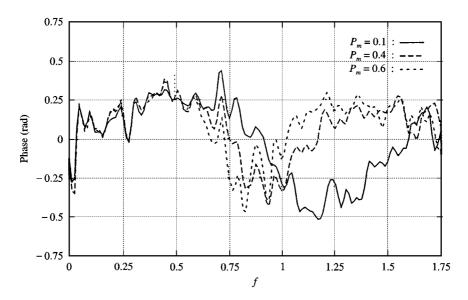
Figure 13. Phase shifts (in rad) between lift coefficients and inflow perturbations in the frequency domain. Parameters are given in Figure 12.

TABLE 3

Evolution of C_L mean value and variance for $P_s = 100$ and $P_g \leq 1$, or $P_s = 500$ and $P_g > 1$. Other parameters are $\alpha = 10°$, $P_m = 0.0$, $\Delta t = 0.02$, $N_e = 10$. Random perturbation of the inflow has the same characteristics as in previous section

P_g	0·97	0·98	0·99	1·00	1·01	1·02	1·05	1·08
P_s	100	100	100	100	500	500	500	500
Mean C_L	0·638	0·689	0·783	0·897	0·882	0·998	1·246	1·429
C_L variance	0·046	0·043	0·053	0·068	0·064	0·068	0·085	0·102

7.3. EFFECT OF P_g

Now, in order to study more precisely the dependence of the sail response on P_g, we fix the mass parameter P_m to 0·0, the load parameter $P_s = 100$ when $P_g \leq 1$ and $P_s = 500$ when $P_g > 1$, and the angle of attack is kept equal to 10°. Time and obstacle discretizations are the same as previously set ($N_e = 10$, $\Delta t = 0.02$). In Figure 14 we compare the spectra of C_L signals for $P_g < 1$ (top) with $P_g > 1$ (bottom). The effect of whether P_g is smaller than 1 or not is clearly evident. When $P_g \leq 1$, high-frequency perturbations are much more filtered than when a length excess exists ($P_g > 1$). Actually, elasticity works in such a way that it absorbs high frequency energy perturbations and releases it at lower frequency in the fluid. Moreover, it is obvious that the system has also some characteristic frequencies at which the energy is transferred from the solid to the fluid domains. We emphasize that as P_g increases, the sets of natural admissible configurations and constant elastic energy displacement fields become larger. As a consequence, the structure can better adapt to the flow for the same elastic energy variations and so the system can respond at higher frequencies.

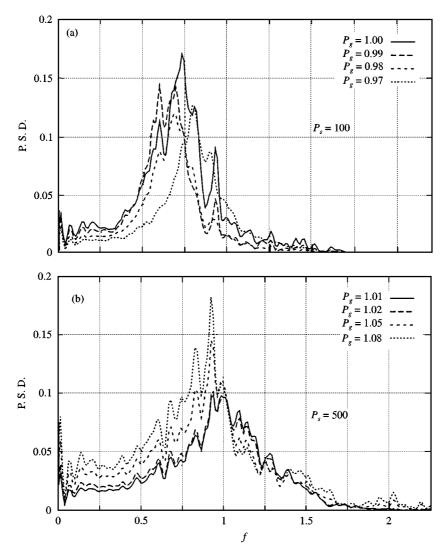Table 3 summarizes the results in terms of mean C_L values and variances.

Figure 14. Comparison of the spectra of C_L signals for various P_g ratios: (a) smaller than 1 and (b) greater than 1, and random perturbations characterized by a variance equal to 0·01 and a spectrum previously reported. Numerical parameters are $N_e = 10$ and $\Delta t = 0.02$. System is defined by $\alpha = 10°$, $P_m = 0.0$, $P_s = 100$ or 500 for (a) and (b), respectively.

7.4. EFFECT OF P_s

Finally, we present the computed C_L spectra for $P_g = 1$ and 1·02 and different values of the load parameter P_s. Table 4 reports the corresponding mean values and variances of the lift coefficients.

As expected, based on the previous results (harmonic perturbations), mean values of C_L as well as variances become larger as P_s decreases. The effect of the load parameter is visible too when analyzing C_L spectra. It is also noted that the shift of the maximum energy peaks (see Figure 15) to higher frequencies, when P_s is increased, is accompanied by an attenuation of the energy level.
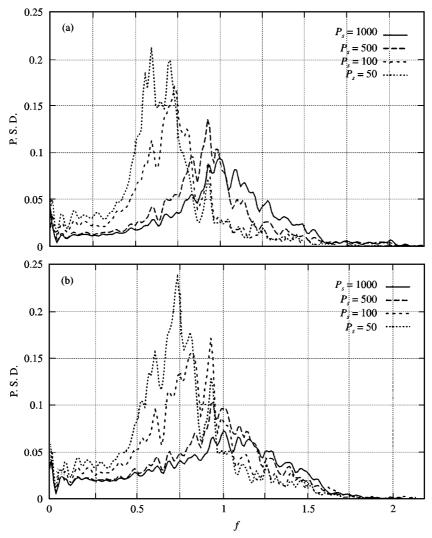
Figure 15. Comparison of the spectra of C_L signals for various load parameters P_s, and (a) $P_g = 1$ and (b) $P_g = 1.02$. Numerical parameters are $N_e = 10$ and $\Delta t = 0.02$. System is defined by $\alpha = 10°$, $P_m = 0.0$. Random perturbations are as defined previously.

TABLE 4

Evolution of C_L mean vlaue and variance for $P_g = 1.00$ and 1.02 and various values of the load parameter P_s. Parameters of the computations are $\alpha = 10°$, $P_m = 0.0$, $N_e = 10$ and $\Delta t = 0.02$. Random perturbation has same characteristics as previously.

| P_s | $P_g = 1.00$ | | $P_g = 1.02$ | |
	Mean C_L	Variance	Mean C_L	Variance
1000	0·682	0·059	0·988	0·064
500	0·724	0·057	0·998	0·068
100	0·897	0·068	1·090	0·089
50	1·022	0·082	1·183	0·102
10	1·597	0·142	1·700	0·161

8. CONCLUSION

The main objective of this work was the analysis of nonlinear coupling between an ideally flexible sail and an unsteady flow. To focus our attention on the effects of large displacements that can easily be realized in common situations (especially when $P_g > 1$), we have developed a simplified theory which relies on an inviscid flow model. The fluid model is then restricted to attached flows and the inviscid flow assumption leads to a vortex sheet representation which only requires a discretization of the solid boundary and of the wake. An interesting feature of the Lagrangian model is that it does not require re-gridding due to the deformation of the obstacle.

The equations of the problem have been established from the inviscid vortex sheet theory on the basis of energy considerations for the complete system including the sail and the flow. While it leads to the same equations as those obtained when the fluid and solid problems are dealt with independently (Le Maître *et al.* 1997a), the global approach is of interest since it yields a better insight into the energy exchanges and provides a natural physical interpretation of the system response.

In the present physical model, the sail response is characterized by three dimensionless parameters. The first two characterize the relative importance of dynamical effects in the fluid and solid domains, while the third is a geometric parameter which quantifies the natural curvature. The influence of these parameters has been analysed in the computations, which focused on the dependence of the sail response to external perturbations. The numerical results have put in evidence the influence of the natural curvature P_g and of the elastic stiffness P_s on the response: as the natural curvature increases, or when the elastic stiffness decreases, the resulting lift coefficient signal exhibits larger variations and eventually nonlinear modes. Moreover, when the inertia of the obstacle is not negligible, a delay between perturbation and response has been observed, which increases with P_m. In the worst cases, P_m can also involve complex responses which present lower frequencies than the perturbation.

To be useful for designers, the problem has now to be extended to three-dimensional situations. The three-dimensional extensions of the models used in this work have already been used for separated three-dimensional computations, for the flow and for the deformation of the sail as well (Charvet 1992; Charvet *et al.* 1997; Le Maître *et al.* 1988, 1997b). The different dynamics of the three-dimensional vortices and the free borders of the sail, in contrast to the prescribed motion of the trailing edge considered here, would probably lead to stronger interactions and more sensitive responses for 3-D cases. However, computational times required to solve the sail equilibrium and the flow are too large to consider a direct unsteady coupling of the codes. Without any insight into the computational time performance, simulation of unsteady three-dimensional responses is not possible using these tools, and future work should focus on this aspect; possibilities include parallel implementations and fast vortex methods.

REFERENCES

ABBOT, I. H. & VON DOENHOFF, A. E. 1958 *Theory of Wing Sections.* New York: Dover.
ANTMAN, S. S. 1995 *Nonlinear Problems of Elasticity,* Vol. 107. New York: Springer Verlag.

BATCHELOR, G. K. 1967 *An Introduction to Fluid Dynamics*. Cambridge: Cambridge University Press.

BATOZ, G. L. & DHATT, G. 1992 *Modélisation des structures par éléments finis*. Paris: Masson.

BERNADOU, M. 1994 *Méthodes d'éléments finis pour les problèmes de coques minces*. Paris: Masson.

BISPLINGHOFF, R. L. & ASHLEY, H. 1982 *Principles of Aeroelasticity*. New York: John Wiley.

BREARD, C. 1996 Modélisation des phénomènes aéroélastiques non linéaires. Thèse de l'Université du Havre.

CHARVET, T. 1992 Résolution numérique de problème liés au comportement des voiles de bateau. Thèse de l'Ecole Polytechnique, Paris.

CHARVET, T., HAUVILLE, F. & HUBERSON, S. G. 1994 Décomposition linéaire/non linéaire d'écoulements instationnaires. *Comptes Rendus de l'Académie des Sciences*, Paris, **318,** Série II: 1019–1026.

CHARVET, T., HAUVILLE, F. & HUBERSON, S. G. 1997. Numerical simulation of real sailing conditions for ship sails flow. *Journal of Wind Engineering and Industrial Aerodynamics* **63,** 111–129.

CHARVET, T. & HUBERSON, S. G. 1992 Numerical calculation of the flow around sails. *European Journal of Mechanics, B* **11,** 599–610.

DOWELL, H., CURTIS, H. C., SCANLAN, R. H. & SISTO, F. 1978 *A Modern Course in Aeroelasticity*. Alphen, The Netherlands: Sijthoff & Noordhe.

FLAY, R., Editor 1997 Special Issue on Sail Aerodynamics. Journal of Wind Engineering and Industrial Aerodynamics **63**.

FUKASAWA, T. & KATORI, M. 1992 Numerical approach to aeroelastic responses of three-dimensional flexible sails. In *The Eleventh Chesapeake Sailing Yacht Symposium*, pp. 87–105.

GUERMOND, J. L. & SELLIER, A. 1991 A unified lifting-line theory. *Journal of Fluid Mechanics*, **229,** 427–451.

JACKSON, P. S. 1985 The analysis of the three-dimensional sails. *Proceedings of the 10th Canadian Congress of Applied Mechanics*, pp. 59–67. University of Western Ontario, Canada.

JACKSON, P. S. & CHRISTIE, G. W. 1986 Numerical analysis of three-dimensional elastic membrane wings. *AIAA Journal* **25,** 676–682.

KATZ, J. & PLOTKINS, A. 1991 *Low-Speed Aerodynamics, from wing theory to Panel Methods*. New York: McGraw-Hill

KREE, P. & SOIZE, C. 1984 *Méchanique aleatorie*. Paris: Dunod.

LE MAÎTRE, O., HAUVILLE, F., HUBERSON, S. G. & SOUZA DE CURSI, J. E. 1997a Aéro-élasticité non linéaire: problème plan pour des obstacles flexibles. In *VI Journée de l'hydrodynamique*. Ecole Centrale Nantes.

LE MAÎTRE, O., HUBERSON, S. G. & SOUZA DE CURSI, J. E. 1997b. Application of a non convex model of fabric deformations to sail cut analysis. *Journal of Wind Engineering and Industrial Aerodynamics* **63,** 77–93.

LE MAÎTRE, O., SOUZA DE CURSI, J. E. & HUBERSON, S. G. 1998 Large displacements analysis for ideally flexible sails. *European Journal of Mechanics. A/Solids* **17,** 619–636.

LEONARD, A. 1980 Vortex methods for flow simulation. *Journal of Computational Physics* **37,** 289–335.

MILNE THOMSON, L. M. (1973) *Theoretical Aerodynamics*. New York: Dover.

ROSENHEAD 1931. The formation of vortices from a surface discontinuities. *Proceedings of the Royal Society of London* A **134,** 170–192.

ROSENHEAD 1932 The point vortex approximation of a vortex sheet. *Proceedings of the Royal Society of London* A **134,** 1041–1081.

SAFFMAN, P. G. 1992. *Vortex Dynamics*, Cambridge: Cambridge University Press.

WILMOTT, P. 1988 Unsteady lifting-line theory by the method of matched asymptotic expansions. *Journal of Fluid Mechanics* **186,** 303–320.

ZIENKIEWICZ, O. C. 1977 *The Finite Element Method in Engineering Sciences*, New York: Mc Graw Hill.